Additive Manufactured Foams for Power Electronics Thermal Management

Student: Justin Broughton
Faculty: Yogendra Joshi

Acknowledgements

- This material is based upon work supported by the U.S. Department of Energy's Office of Energy Efficiency and Renewable Energy (EERE) under the Vehicle Technologies Program Office Award Number DE-EE0008708.
- Support from Haipeng Qiao and Prof. Christopher Saldana with the tomographic imaging is also appreciated.

- **Disclaimer:** This report was prepared as an account of work sponsored by an agency of the United States Government. Neither the United States Government nor any agency thereof, nor any of their employees, makes any warranty, express or implied, or assumes any legal liability or responsibility for the accuracy, completeness, or usefulness of any information, apparatus, product, or process disclosed, or represents that its use would not infringe privately owned rights.

1. Introduction

1.1 Wide-bandgap devices and motivation

- Wide-bandgap (WBG) devices have higher efficiencies, withstand higher breakdown voltages, can operate at increased switching frequencies, and function at higher temperatures
- Devices seeing mass commercialization and implementation in high voltage applications
- Design for WBG leads to miniaturization and potential hotspots
- Reexamination of thermal management needed for smaller devices and systems

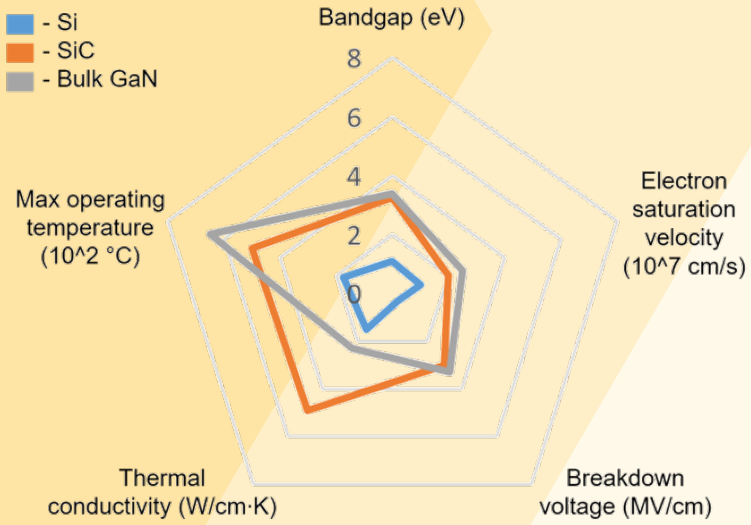

Figure 1: Material properties of power semiconductors

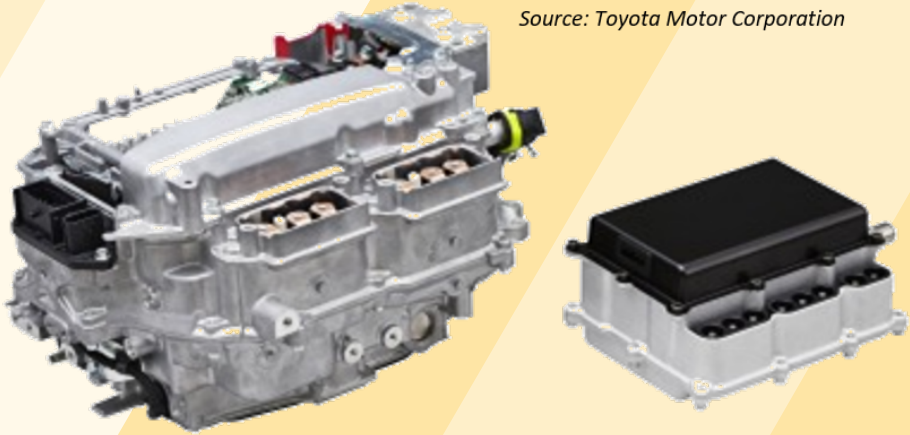

Source: Toyota Motor Corporation

Left: PCU with silicon power semiconductors (Production model)
Right: PCU with SiC power semiconductors (Future Target)

Figure 2: Miniaturization potential with system-level redesign using WBG devices

1. Introduction

1.2 Metal foams and additive manufacturing

- Open-cell foams - interconnecting nodes and ligaments with high porosity, tortuous flow paths, and high specific surface area (SSA)
- Metal foams are used in applications ranging from catalysts for chemical reactions, impact absorption, and heat transfer
- Additive manufacturing (AM) has been used for foam-type structures, but not the combination between AM and metal foams is relatively unexplored
- Present work investigates the thermo-hydraulic performance of both traditionally manufactured metal foams and AM foams as a method of heat transfer enhancement

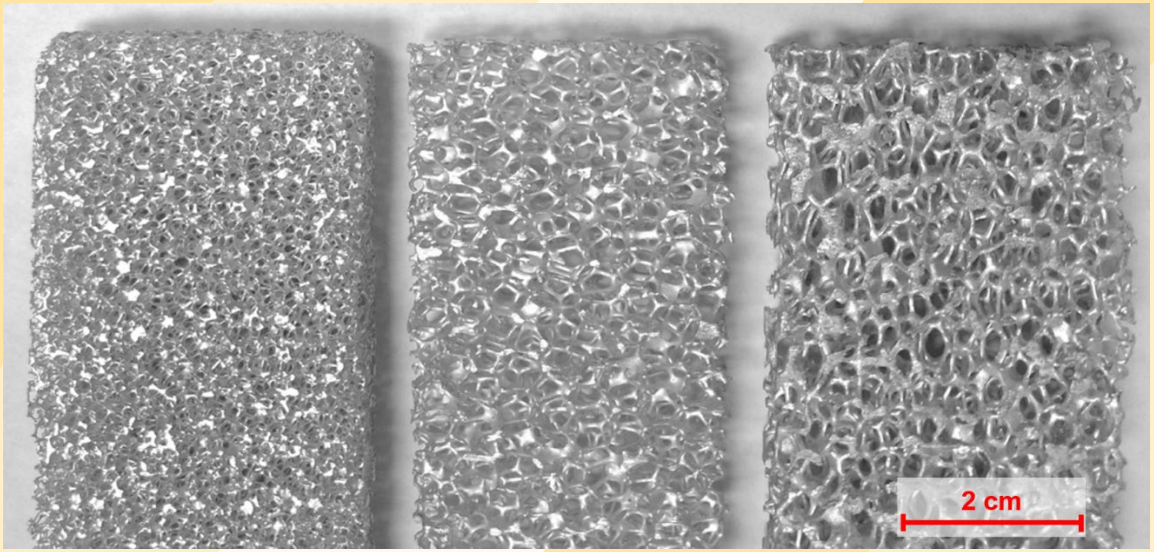

Figure 3: Photograph of metal foams of various sizes purchased from ERG Aerospace, Inc.

2. Characterization and sample descriptions

2.1 Characterization methodology, unit cell selection

- 5 PPI, processed from 6101 alloy, and underwent T6 heat treatment
- Zeiss Metrotom 800 for x-ray µCT (scanned at 0.25˚ rotations, 18.43 µm voxel size)
- ImageJ/BoneJ used for image analysis

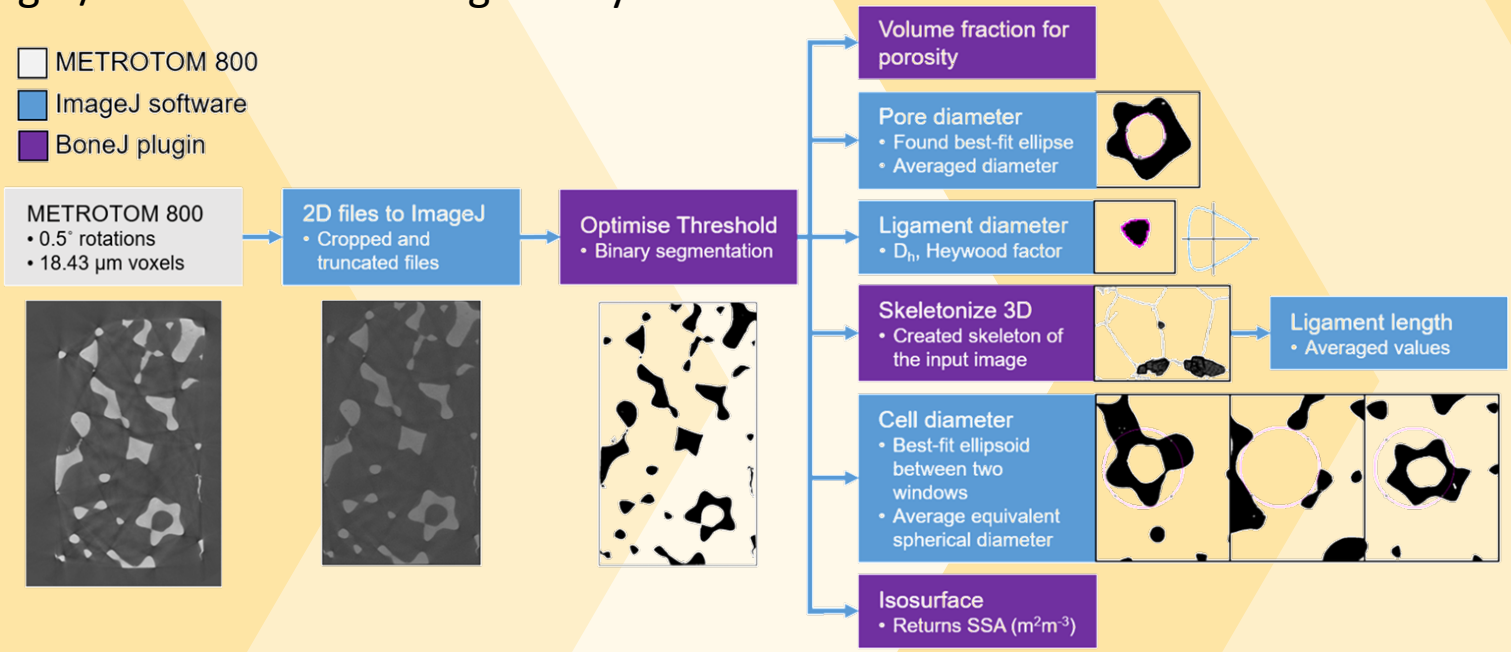

Figure 4: Illustration of steps for commercial stochastic foam characterization.

- Rhombic dodecahedron unit cell chosen for this work

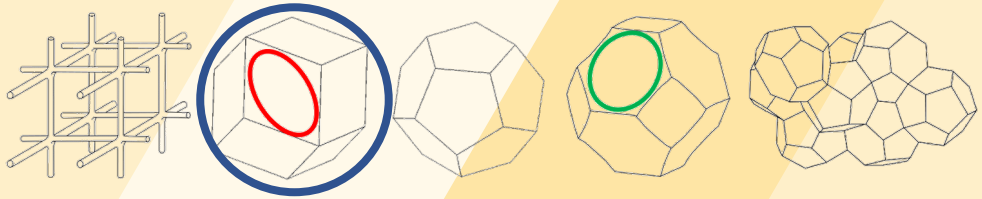

Figure 5: Types of unit cells seen in literature.

2. Characterization and sample descriptions

2.2 Unit cell description and experimental test samples

- AM unit cell seen in figure 4
- Unit cell based on porosity and cell diameter
- Reasonable agreement for most properties between result, literature, and rhombic dodecahedron unit cell
- ERG foam bonded with Omegabond 200 Epoxy Adhesive (k = 1.38 W/m•K, thickness 0.3 mm) to aluminum substrate

Table 1: Comparison of foam properties from x-ray μCT analysis, literature, and AM foam.

Parameter	Result	Literature comparison	Rhombic dodecahedron
PPI	5	5	5
Porosity	86.5%	92%	86.5%
Ligament diameter (mm)	0.508	0.505	0.548
Ligament length (mm)	1.94	1.72	2.014
Pore diameter (mm)	2.58	2.61	1.35
Cell diameter (mm)	4.65	4.60	4.65
Surface area (m^2m^{-3})	571.1	510	927.35

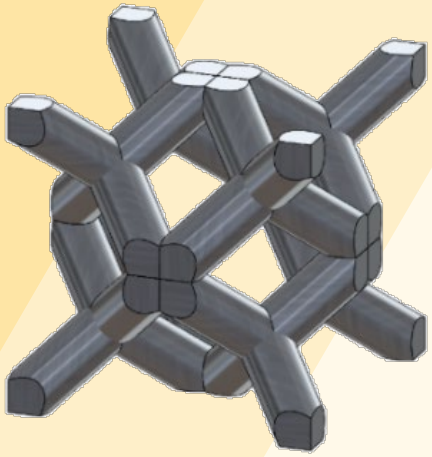

Figure 6: Dimetric and diagonal views of a rhombic dodecahedron based unit cell.

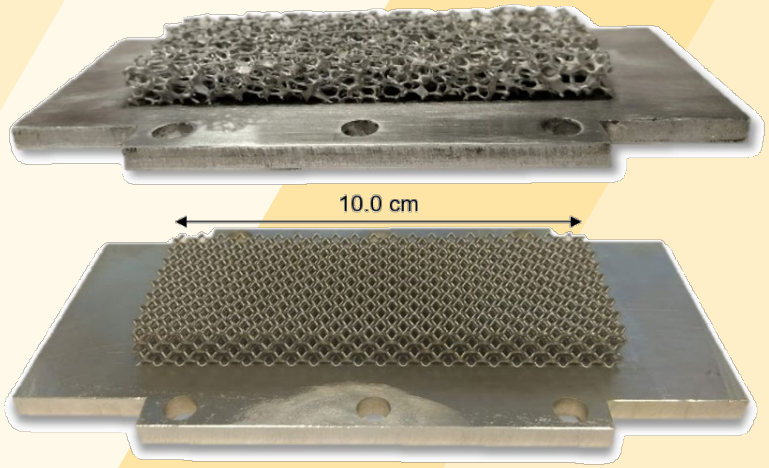

Figure 7: Stochastic ERG foam with visible thermal epoxy layer (top) and designed foam (bottom)

3. Model and experimental setup

3.1 Computational model description and assumptions

- *Isosurface* command in ImageJ to export stochastic STL file
- Dimensions: 9.30 mm x 4.65 mm x 25.0 mm and 9.30 mm x 2.33 mm x 46.5 mm
- Assumptions:
  - Representative elementary volume (> 8 unit cells for REV)
  - Minimal inlet effects (valid at lower speeds)
  - Steady state, laminar (Re_K = 37.5), incompressible flow with negligible viscous dissipation
- Thermal resistance from thermal epoxy included into simulation results

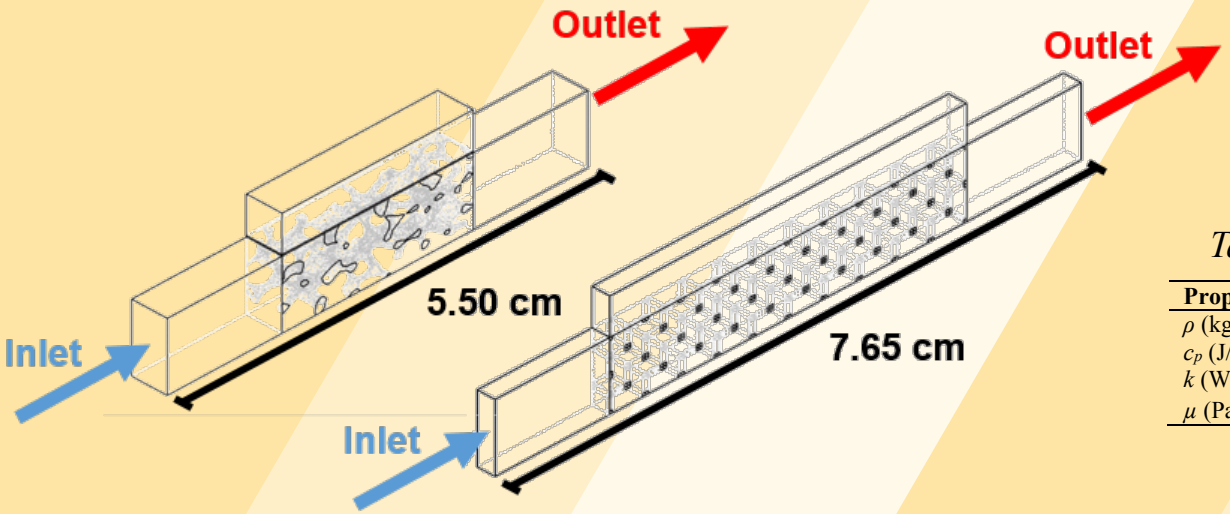

Figure 9: Reduced ERG sample geometry with TIM (left) and reduced AM geometry (right) used in computational studies.

Table 2: Material properties at 25 ˚C .

Property	Al 6101	AlSi10Mg	Al 5083	Water
ρ (kg/m^3)	2700	2670	2660	998
c_p (J/kg•K)	896	890	900	4182
k (W/m•K)	167	173	117	0.6
μ (Pa•s)	-	-	-	0.001003

3. Model and experimental setup

3.2 Experimental testing setup and procedures

- Working fluid: degassed, deionized (DI) water
- Equipped with type-T thermocouples and several pressure transducers
- Uniform heat flux heating condition achieved with a heater block
- Test samples were nominally 4 cm x 10 cm x 0.93 cm
- Heated section area of 4 cm x 10 cm

Table 3: Experimental uncertainties.

Parameter	Uncertainty
Pressure	±20 Pa
Flow rate	±4 mL/s
Temperature (type T thermocouple)	±0.5 K
Heat flux (heater block)	±0.2 W/cm^2

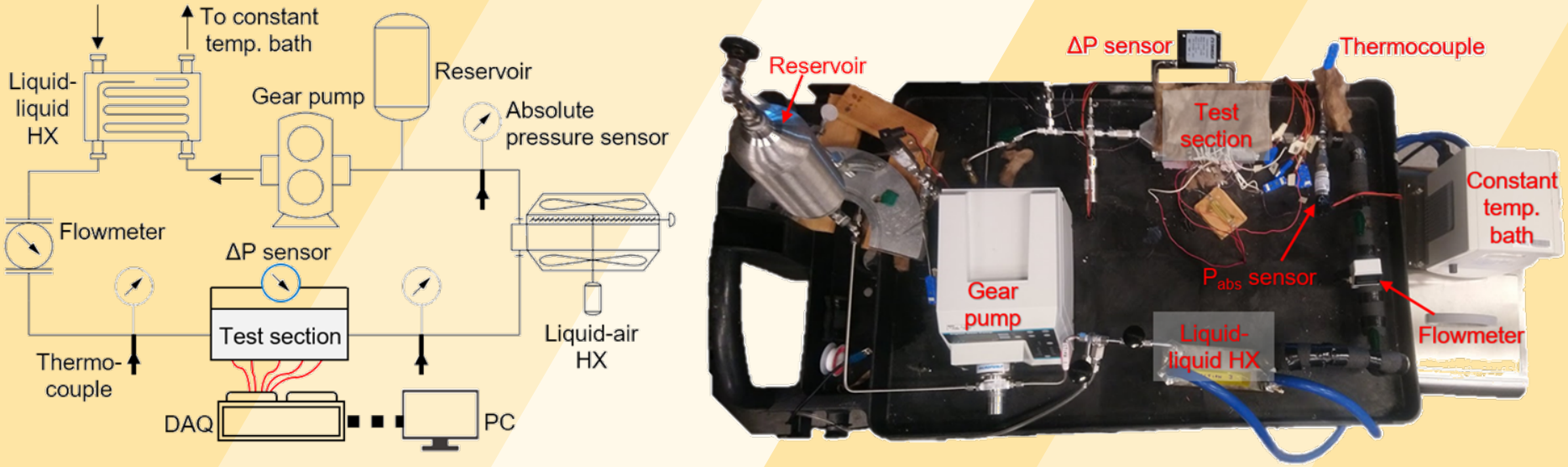

Figure 10: Closed flow loop and data acquisition setup.

4. Results

4.1 Thermohydraulic validation

- Validation before using computational models for further analysis
- Comparing total pressure drop across test section and effective Nusselt number
- Results fit to a second-order polynomial (Darcy-Forchheimer Law) and power law fit
  Good agreement between experimental and numerical results
- Pressure drop is higher (66%) for the AM sample, but the penalty comes with approximately 60% increase in effective heat transfer coefficient

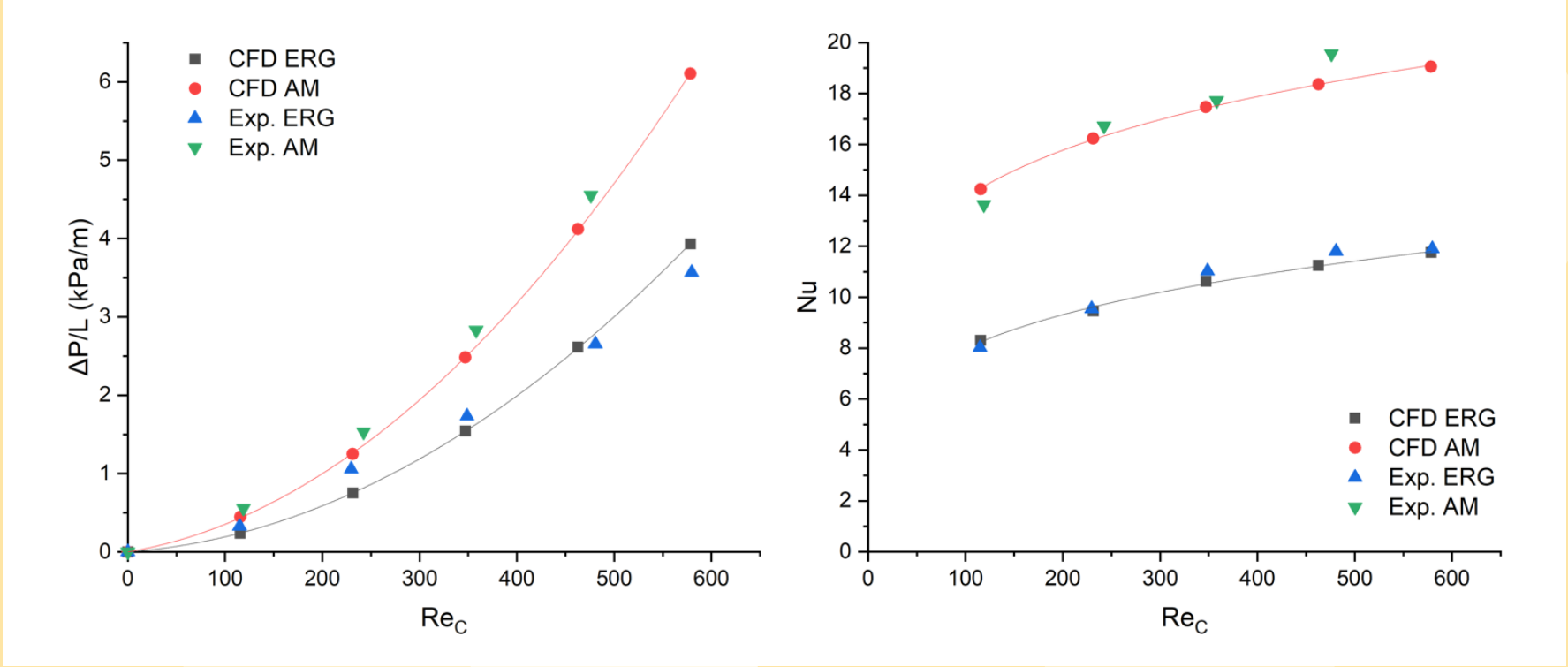

Figure 11: Reduced ERG sample geometry with TIM (left) and reduced AM geometry (right) used in computational studies.

4. Results

4.2 Streamlines analysis for flow tortuosity studies

- Dispersion conductivity k_d accounts for pore-scale mixing in volume-averaged simulations
- Calmidi and Mahajan: $k_d = C_D \rho u \sqrt{K} c_P$
- Tortuosity defined as $\tau = {}^{s}/_{L}$
  - s is the total distance traveled
  - L is the shortest travel length possible
- Additional example correlation:

$$\frac{k_d}{k_f} = c(\tau - 1)\left(1 - \frac{\varepsilon}{\tau}\right) Re_p Pr$$

- Tortuosity values were calculated as 1.093 and 1.038, respectively
- Implies that commercial foam has higher thermal dispersion conductivity
- Further studies regarding k_d for either structure type should be undertaken

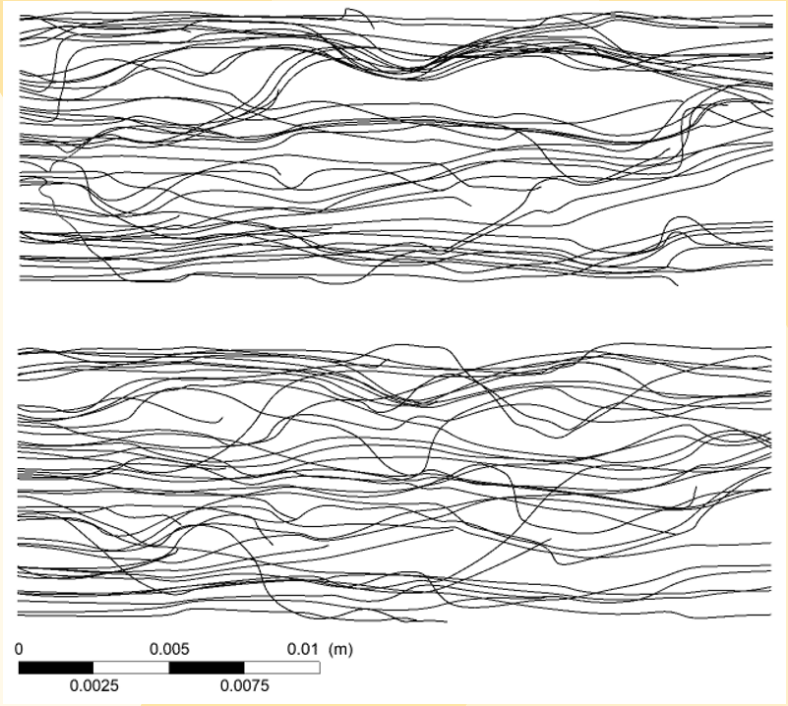

Figure 12: Streamlines visualized for stochastic geometry with u = 2.5 cm/s (top) and u = 10 cm/s (bottom)

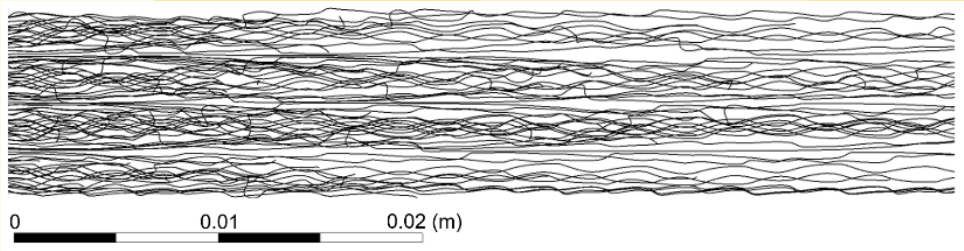

Figure 13: Designed sample streamlines for u = 10 cm/s.

4. Results

4.3 Velocity and pressure contours

- Random vs. ordered flow patterns
- Existence of large stagnant zones in the commercial sample (with relative lack of such large low velocity zones in the AM geometry)

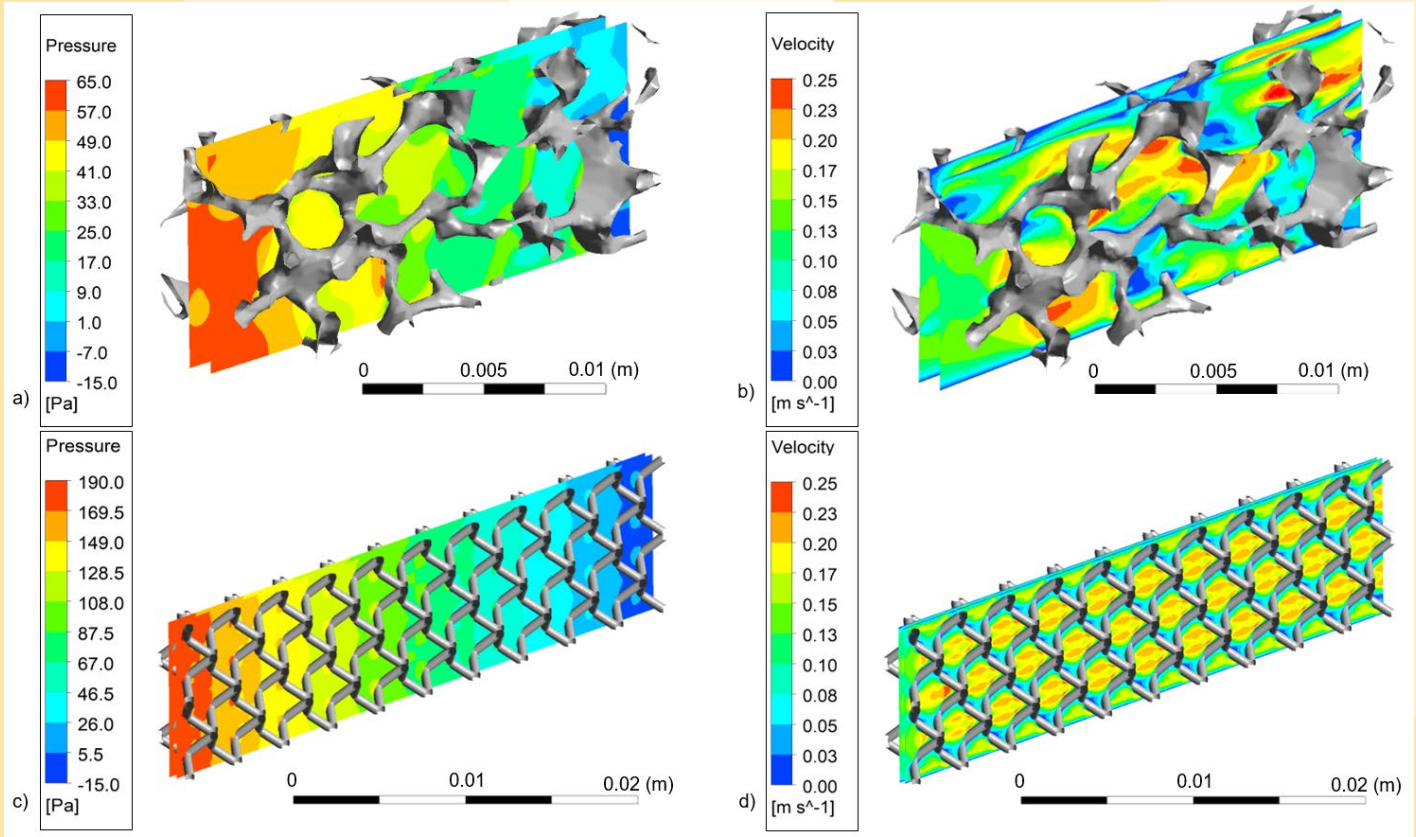

Figure 14: Flow fields for u = 10 cm/s for the commercial and AM foams a) Pressure contours, b) Velocity contours, c) Pressure contour, and d) Velocity contour for AM.

4. Results

4.4 Resistor network for thermal interface material analysis

- Quantifying reasons for performance improvement – structural differences in the foam vs. elimination of the TIM
- U_{new} calculated for three k_{TIM} values (k_{TIM} = 4.0, 40, and ∞ W/m•K to represent high conductivity epoxy, a solder, and no TIM layer)
- $U_{new} = \left[\frac{1}{U_{k=1.38}} - \frac{t_{TIM}}{k_{original}} + \frac{t_{TIM}}{k_{new}}\right]^{-1}$
- 1D resistor network validated with k = 4.0 W/m•K results
- Incrementally improving k_{TIM} has a large impact at lower values but not so much at higher k values
- Performance of the commercial foam approaches AM foam with increasing flow speeds, which may be caused by the differences in k_d

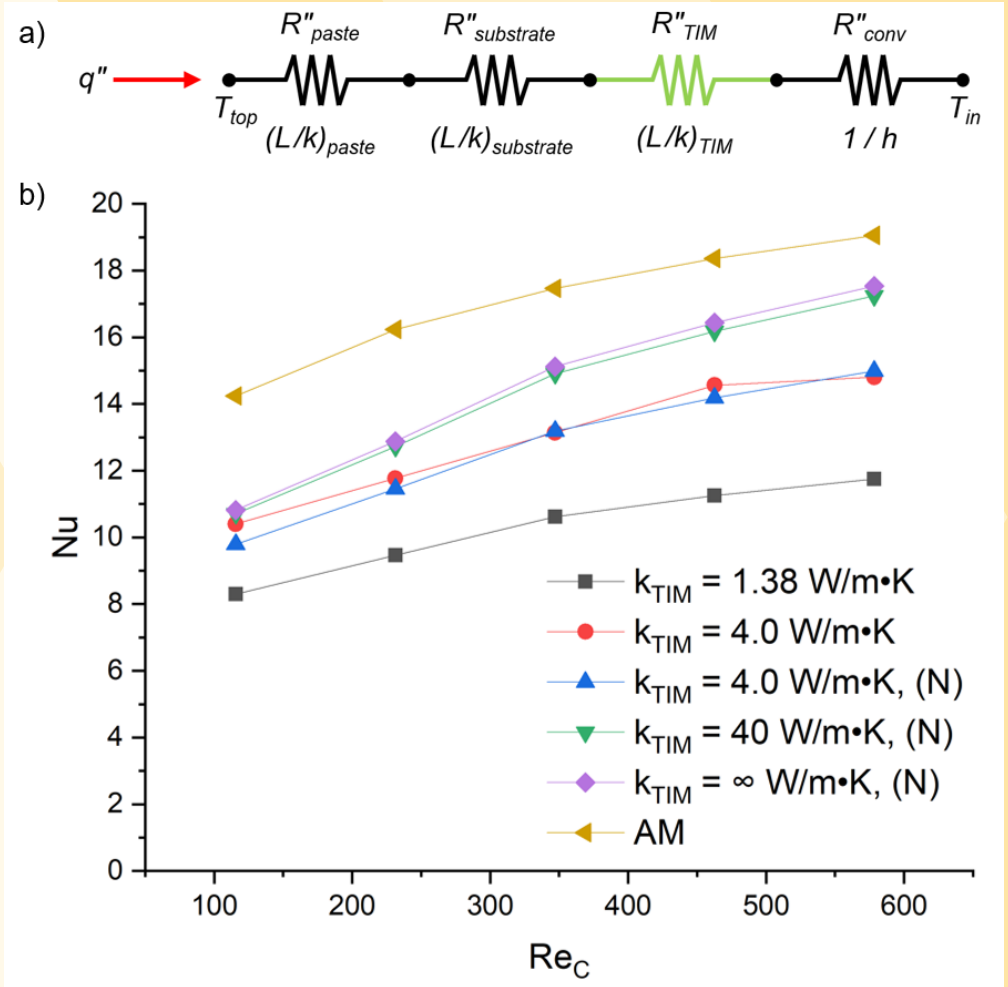

Figure 15: Non-dimensional heat transfer performance for AM foam and ERG Inc. foam with varying k_{TIM} values – (N) denotes values found using a resistance network approach.

4. Results

4.5 Interfacial heat transfer coefficient and fin efficiency analysis

- Interfacial heat transfer coefficient (h_{sf}) is important for volume-averaged CFD simulations
- Calmidi and Mahajan: $Nu_{sf} = \frac{h_{sf} d_l}{k_f} = 0.52 Re_l^{0.5} Pr^{0.37}$
- Hunt and Tien: $Nu_{sf} = \frac{h_{sf} d_l}{k_f} = 0.418 Re_l^{0.53} Pr^{1/3}$
- Reasonable but not good agreement between correlations and numerical results
- Commercial foam has better fin efficiency except at lower inlet velocities – but this is due to the fact that the isothermal simulation convects much more heat for the AM model

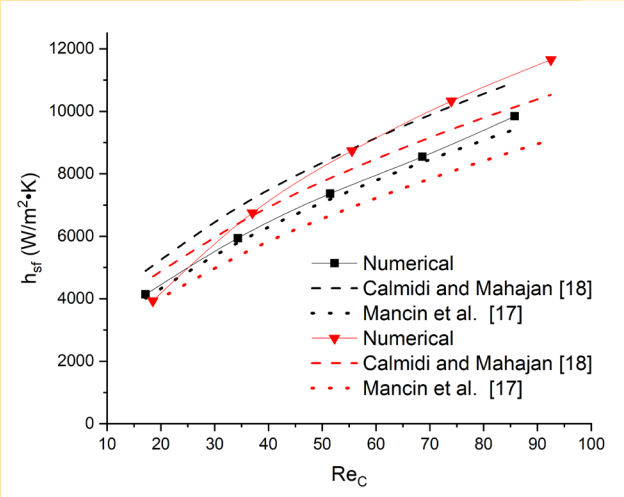

Figure 16: Comparison of numerical results and correlations results for commercial and AM foam

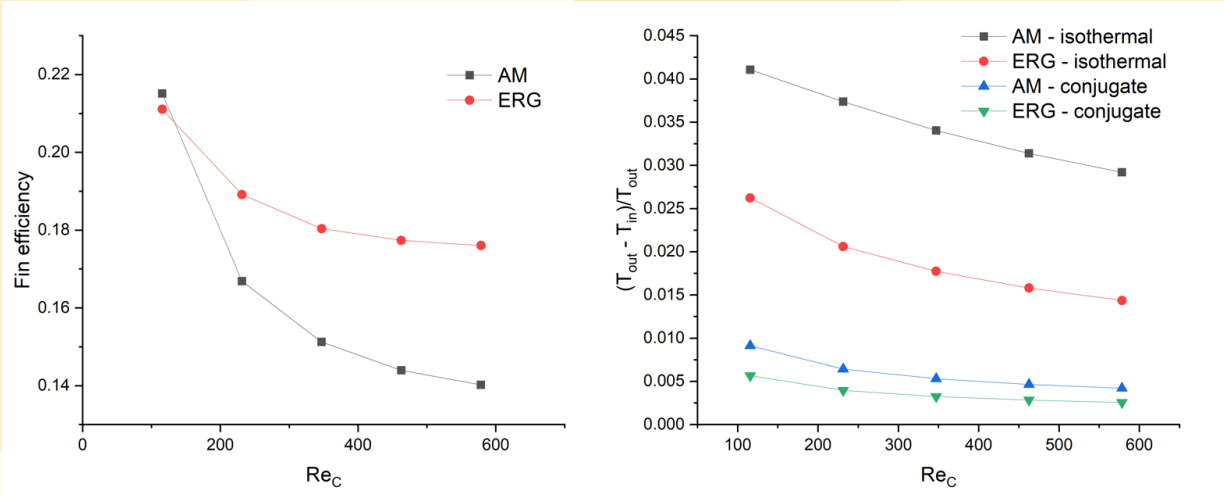

Figure 17: Fin efficiency for a 2.5 cm sample length (left) and nondimensionalized outlet temperature comparison for constant and variable ligament temperature (right).

5. Conclusions

- Demonstrated the advantages of traditionally manufactured and AM metal foams for thermal management
- Analyzed using commercial CFD-HT software, validated computational models
- Tortuosity results suggests that k_d should be adjusted for the AM structure
- Commercial foams would be viable if k_{TIM} values could be increased
- Interfacial heat transfer coefficients were shown to agree somewhat with correlations found in literature

Research Focus	2020				2021			
	Q1	Q2	Q3	Q4	Q1	Q2	Q3	Q4
Sample fabrication			Pressure mitigating structure					
Testing in flow loop					Pressure mitigating structure			
Conjugate heat transfer modeling	Pore scale boiling model		2 phase VA models			New structure 2 phase VA model validation		